JOURNAL OF GEOPHYSICAL RESEARCH, VOL. 99, NO. A6, PAGES 11,265–11,276, JUNE 1, 1994

Electron inertial effects on geomagnetic field line resonances

C. Q. Wei, J. C. Samson, R. Rankin, and P. Frycz

Canadian Network for Space Research, University of Alberta, Edmonton, Canada

Abstract. A three-dimensional compressible resistive magnetohydrodynamic simulation code, with inclusion of the fully generalized Ohm's law, has been developed to study the nonlinear evolution of field line resonances in Earth's magnetosphere. A simple Cartesian box model of an inhomogeneous plasma with straight geomagnetic field lines is used, and the Alfvén velocity increases monotonically from the magnetopause boundary layer toward Earth. A monochromatic fast mode compressional oblique wave is applied from the direction of the magnetopause boundary layer, pumping energy into the magnetosphere. The fast mode wave, while propagating toward Earth, is partially reflected at the turning point (located at radial distances between 8 and 10 R_E in the equatorial plane) and then couples to shear Alfvén waves, leading to the formation of large-amplitude field line resonances near Earth. The field line resonances are observed to narrow to several electron inertia lengths within several wave periods of the driver wave, and electron inertial effects become important at this stage. Final profiles near the resonance are very similar to Airy functions, indicating that electron inertial effects become important before possible nonlinear effects. The electron inertial effects lead to oscillating parallel electric field which might be potential accelerators for electrons in some types of auroral arcs.

1. Introduction

Fluctuations, particularly solar wind pressure pulses, are important external sources of ultralow frequency magnetohydrodynamic (MHD) waves in the terrestrial magnetosphere [*Southwood and Hughes*, 1983; *Yumoto*, 1988; *Allan and Poulter*, 1992; *Lee and Wei*, 1993]. Some observations of monochromatic ultralow frequency waves [e.g., *Cummings et al.*, 1969; *Samson*, 1972] have been interpreted as standing shear Alfvén waves or field line resonances (FLRs). A number of theories have been developed to explain the coupling of compressional energy to the shear Alfvén waves and the formation of monochromatic compressional modes in magnetospheric cavities [*Chen and Hasegawa*, 1974a, b; *Southwood*, 1974; *Hasegawa and Chen*, 1976; *Allan et al.*, 1986; *Kivelson and Southwood*, 1985; *Zhu and Kivelson*, 1988; *Lee and Lysak*, 1989, 1991; *Harrold and Samson*, 1992].

Field line resonances might play a direct role in controlling the formation of some auroral arcs [*Samson et al.*, 1991; *Walker et al.*, 1992; *Xu et al.*, 1993]. If the resonance is narrow enough, kinetic Alfvén waves [*Hasegawa*, 1976; *Goertz*, 1984] or inertial Alfvén waves [*Lysak*, 1990; *Seyler*, 1990] can give rise to electric field components parallel to the ambient magnetic field. These parallel electric field components may accelerate electrons and lead to the spatial modulation of small-scale auroral arcs. *Walker et al.* [1992] analysed data from the Goose Bay HF radar and found that at the ionosphere the FLR width can be less than 40 km, which is actually the lower limit of the radar resolution, and that smaller scale structures are also possible. Satellite observations of FLRs have revealed that their widths at the equatorial plane can be as small as 0.2 R_E (R_E = 6400 km, the Earth's radius) [*Hughes et al.*, 1978; *Singer et al.*, 1982], which could map to ~ 30 km in the auroral ionosphere. Analytical and computational models [*Walker et al.*, 1982; *Rankin et al.*, 1993b] show that the FLRs have spatial scales in the fields which are substantially smaller than the resonance width. The 180° radial phase shift through the resonance leads to spatial scales or shears in the azimuthal magnetic field that are about one fifth the width of the resonance [*Rankin et al.*, 1993b].

Electron inertial effects on FLRs have been investigated previously by using other approaches. *Inhester* [1987] obtained computational solutions of the linear MHD equations and found that either kinetic Alfvén waves or inertial Alfvén waves may lead to modification of the FLR structure. In computational studies of small-scale discrete auroral arcs, *Seyler* [1990] used an incompressible model with inclusion of the dispersive effect of electron inertia and concluded that electron inertia can significantly affect the formation of small-scale auroral arcs.

Recently, *Rankin et al.* [1993b] carried out a three-dimensional compressible MHD simulation to study the evolution of standing wave FLR in the nightside magnetosphere. They found that the resonant mode conversion of energy from compressional waves to shear Alfvén waves may lead to FLR widths small enough to allow kinetic or electron inertial effects.

In the present work, the recent study of the nonlinear evolution of FLRs [*Rankin et al.*, 1993b] has been extended to include finite electron inertial effects. To study the electron inertial effect together with the FLR, we have developed a model for the three-dimensional nonlinear evolution of FLRs in Earth's magnetosphere by including the dispersive effect of electron inertia in the generalized Ohm's law. Though nonlinear effects do not dominate our

Paper number 94JA00582.
0148-0227/94/94JA-00582$05.00

simulation, it is very important that the computational code be able to handle possible nonlinear effects. For example, nonlinear harmonic generation in the standing Alfvén wave can lead to a number of possible effects including ponderomotive forces [*Allan*, 1992] and cascading of wave energy to higher harmonics. Generation of these harmonics would severely influence the development of inertial Alfvén waves. In our model, a simple box geometry of an inhomogeneous plasma with straight geomagnetic field lines is used, and the Alfvén velocity increases monotonically from the magnetopause toward Earth. A fast mode compressional oblique wave is applied from the direction of the magnetopause boundary layer, pumping energy into the magnetosphere. The fast mode incident wave, while propagating toward Earth, is partially reflected at the turning point and, with appropriate choices of the wave vector, the coupling of fast mode waves to shear Alfvén waves leads to the formation of large-amplitude FLRs nearer the Earth. We find that the dispersive effect of electron inertia becomes important in the resonance structures when the resonance narrows to several electron inertia lengths. Final profiles near the resonance are very similar to the Airy function solutions which are typical of mode conversion.

In section 2 we describe the simulation model and the governing equations, including a generalized Ohm's law with electron inertia. We also consider the linearized equations and the form of the FLRs in the linear regime as well as the dispersion relation derived from the MHD equations with the generalized Ohm's law. The simulation results for cases both with and without electron inertial effects are presented in section 3, together with their comparisons. Our results show that for the configuration we are considering, electron inertial effects play the major role in the evolution of the FLRs, with little, if any, influence from nonlinear effects such as harmonic generation. Section 4 contains a discussion of our simulation results and their possible implications in interpreting observations as well as a summary of the simulation results.

2. Simulation Model and Governing Equations

In this section we present the simulation model for our study of electron inertial effects including the governing equations, the simulation domain, the numerical scheme, and the boundary conditions. In addition, in order to clarify our interpretation of the simulation results, we also present the linear theory of FLRs and derive the linear dispersion relationship for the MHD equations with the electron inertial term.

As solar wind disturbances, such as pressure pulses, reach the magnetopause, the solar wind energy can be transported into the magnetosphere in the form of fast compressional waves. These waves propagate deep into the magnetosphere and possibly form cavity modes between the surface of the turning point and the magnetopause [*Allan et al.*, 1986; *Kivelson and Southwood*, 1986; *Zhu and Kivelson*, 1988]. These compressional cavity modes form at discrete frequencies and are the source of the monochromatic compressional drivers for the FLRs [*Chen and Hasegawa*, 1974a, b; *Southwood*, 1974]. The fast mode wave is only partially reflected at the turning point, and some portion of the wave energy evanescently decays Earthward of the turning point. When the frequency of the fast mode wave matches the frequency of the local shear Alfvén wave (resonant point), mode coupling can occur, and the energy is converted irreversibly from the fast mode to the shear Alfvén mode, leading to the resonant excitation of FLRs.

In order to simplify our computational scheme, we do not include a full cavity mode scenario but use a monochromatic fast mode driver, propagating inward from the magnetopause. Our simulation includes both the turning point and the resonance, but to save on computing time, the simulation box has a boundary just outside the turning point.

Note that two scale lengths are involved in the above description, namely, the large scale length of the whole magnetosphere and the small scale length of the electron inertia. The scale size of the whole magnetosphere is of the order of 10 R_E, while typical electron inertia lengths are only several kilometers for typical plasma densities in the magnetosphere. Therefore a model which is valid on both the scale size of the whole magnetosphere and the scale size of the electron inertia length is required for the study of the dispersive effects of electron inertia on the nonlinear development of driven FLRs. Computationally, it is very difficult to have spatial resolution on the electron inertia scale while also studying global magnetospheric phenomena. In addition, because of the complexity of the magnetospheric system, we neglect the curvature of the geomagnetic field so that the convergence of the magnetic field and the decreased thickness of the FLRs near the ionosphere (where electron inertial effects are likely to be important) are not part of our model. In order to accommodate the very different scale sizes, we have chosen a compromise configuration for our simulation. We consider a relatively small "box" model with most of the essential ingredients including a nonuniform magnetospheric plasma, reflecting ionospheres, and the surfaces of the turning points and the resonances for the fast mode monochromatic driver.

To include electron inertia in the global magnetospheric system, the governing equations to be used consist of the full set of resistive MHD equations with inclusion of the electron inertial term in the Ohm's law.

$$\frac{\partial \rho}{\partial t} = -\nabla \cdot (\rho \mathbf{v}) \tag{1}$$

$$\rho \frac{\partial \mathbf{v}}{\partial t} = -\rho \mathbf{v} \cdot \nabla \mathbf{v} - \nabla P + \mathbf{J} \times \mathbf{B} \tag{2}$$

$$\frac{\partial \mathbf{B}}{\partial t} = -\nabla \times \mathbf{E} \tag{3}$$

$$\nabla \times \mathbf{B} = \mu_0 \mathbf{J} \tag{4}$$

$$\mathbf{E} + \mathbf{v} \times \mathbf{B} = \frac{m_e}{ne^2} \frac{\partial \mathbf{J}}{\partial t} + \eta \mathbf{J} \tag{5}$$

$$\frac{\partial P}{\partial t} = -\mathbf{v} \cdot \nabla P - \gamma P \nabla \cdot \mathbf{v} + (\gamma - 1)\eta \mathbf{J}^2 \tag{6}$$

where ρ is the plasma density, $\mathbf{v}$ is the flow velocity, P is the total plasma pressure, $\mathbf{J}$ is the total current, $\mathbf{B}$ is the magnetic field, $\mathbf{E}$ is the electric field, μ_0 is the permeability in vacuum, m_e is the electron mass, e is the electron charge, η is the magnetic resistivity, and γ is the ratio of specific heats ($\gamma = 5/3$).

Equation (5) is an Ohm's law which includes the electron inertial term beyond the so-called resistive MHD case. The last term on the right-hand side is the magnetic resistivity term, which gives magnetic diffusion effects. The electron pressure (or high temperature) term is ignored because in this paper we have chosen to model the effects of driving FLRs in a low β ($\beta \ll m_e/m_i$) plasma, such as might be seen at 1.5 or 2 R_E altitude. On the other hand, in the magnetosphere the pressure term probably becomes important near the equatorial plane where the plasma will have finite β. Other terms, such as the ion inertial (or Hall) term and the nonlinear electron inertial terms have also been ignored.

The above set of equations is in a dimensional form. In the numerical simulation, these equations can be put into a dimensionless form by using appropriate normalizations. In the present study the length is normalized by a characteristic length a, the number density by the plasma number density at the left boundary of the simulation box N_0, the plasma density by $m_i N_0$, the magnetic field by the magnetic field at the left boundary B_0, the velocity by the Alfvén velocity at the left boundary V_{A0}, and the time by the characteristic Alfvén transit time $t_A \equiv a/V_{A0}$. The normalization of the thermodynamic quantities is chosen such that $P_0 = B_0^2/2\mu_0 = \rho_0 V_{A0}^2/2$. The magnetic Reynolds number is defined as $R_m = \mu_0 V_{A0} a/\eta$. With the above normalizations and some straightforward mathematical operations, (1) – (6) can be expressed in dimensionless form as

$$\frac{\partial \mathbf{\Gamma}}{\partial t} - \nabla \times (\mathbf{v} \times \mathbf{B} - \nabla \times \mathbf{B}/R_m) = 0 \quad (7)$$

$$\frac{\partial(\rho \mathbf{v})}{\partial t} + \nabla \cdot (\rho \mathbf{v}\mathbf{v}) + \frac{1}{2}\nabla P + \mathbf{B} \times (\nabla \times \mathbf{B}) = 0 \quad (8)$$

$$\frac{\partial \rho}{\partial t} + \nabla \cdot (\rho \mathbf{v}) = 0 \quad (9)$$

$$\frac{\partial P}{\partial t} + \nabla \cdot (\gamma P \mathbf{v}) - (\gamma - 1)[\mathbf{v} \cdot \nabla P + 2(\nabla \times \mathbf{B})^2/R_m] = 0 \quad (10)$$

where

$$\mathbf{\Gamma} \equiv \mathbf{B} + \nabla \times (\lambda_e^2 \nabla \times \mathbf{B}) \quad (11)$$

and $\lambda_e = (m_e/\mu_0 n e^2)^{1/2}/a$ is the normalized collisionless skin depth due to electron inertia (or the electron inertia length). If we set the electron inertia length to zero, (7) – (10), together with (11), will be the same as the simple resistive MHD equations.

Equations (7) – (10) are a set of eight equations in eight unknowns $\mathbf{\Gamma}$, $\rho \mathbf{v}$, ρ, and P. Only (9) is in a conservation form. Equation (8) could be converted to a conservation form by adding an extra term $\mathbf{B}(\nabla \cdot \mathbf{B}) = 0$. However, this conversion would add a pseudoforce to the equation and affect the accuracy of velocity calculations because $\nabla \cdot \mathbf{B}$ is not necessarily zero on a finite difference mesh [e.g., *Finan and Killeen*, 1981]. The advantage of using a nonconservation form for (10) is that the pressure is the main variable, which is especially useful when processes in low β plasmas are simulated. Equation (7) is in a pseudovector conservation form even with inclusion of electron inertia.

Before going to the detailed numerical studies, we present some linear theoretical analyses based on (1) – (6) to serve as a basis for the discussion of the numerical study. First, we derive the equation for perturbed components in order to find the turning points and the resonances in our model of a nonuniform magnetoplasma. Since we are mainly concerned about the approximate positions of the turning points and the resonances rather than details of the resonance structure, for simplicity we temporarily neglect the electron inertial effect. Assuming that the ambient magnetic field is along the z direction and the plasma density, pressure, and magnetic field vary only along the x direction (radially toward Earth), we can proceed to linearize (1) – (6). If we define the displacement vector ξ by $\mathbf{v}_1 = \partial\xi/\partial t$, where $\mathbf{v}_1$ is the perturbed velocity and take the displacement vector to have the form $\xi(\mathbf{x}, t) = \xi(x) \exp [i(k_y y + k_z z - \omega t)]$, it can be shown that, by inserting the displacement vector into (1) – (6), the x component of the displacement can be expressed as [e.g., *Roberts*, 1984]

$$\frac{d}{dx}[\rho_0(c_s^2 + V_A^2)A\frac{d\xi_x}{dx}] + \rho_0(\omega^2 - k_z^2 V_A^2)\xi_x = 0 \quad (12)$$

where

$$A \equiv \frac{(\omega^2 - k_z^2 V_A^2)(\omega^2 - k_z^2 c_T^2)}{(\omega^2 - \omega_f^2)(\omega^2 - \omega_s^2)}$$

$$\omega_f^2 + \omega_s^2 = K^2(c_s^2 + V_A^2) \qquad \omega_f^2 \omega_s^2 = K^2 k_z^2 c_s^2 V_A^2 \quad (13)$$

$$K^2 = k_y^2 + k_z^2 \qquad c_T^2 = \frac{c_s^2 V_A^2}{c_s^2 + V_A^2}$$

where c_s is the sound speed, w_f is the fast mode frequency, and w_s is the slow mode frequency.

It can be seen from the expression for A in (13) that expression (12) has two singularities, namely, $\omega = \omega_f$ and $\omega = \omega_s$. These two singularities give the turning points. In addition, expression A also has two resonances, $\omega^2 = k_z^2 V_A^2$ and $\omega^2 = k_z^2 c_T^2$, where the compressional wave couples its energy into the shear wave and the slow mode "cusp" resonance. In a cold plasma, $c_T = c_s = 0$ and $\omega_s = 0$, only one turning point and one resonance exist. The turning point is located at $\omega^2 = (k_y^2 + k_z^2)V_A^2(x_t)$, and the resonance is located at $\omega^2 = k_z^2 V_A^2(x_r)$, where x_t and x_r represent the positions of the turning point and the resonance, respectively.

The linear dispersion relationship for the MHD equations with electron inertia can also be obtained by assuming the perturbation has the form $f_1(\mathbf{x}, t) = f \exp [i(k_\perp x + k_z z - \omega t)]$, where $\mathbf{k} = k_\perp \hat{\mathbf{x}} + k_z \hat{\mathbf{z}}$ and $k^2 = k_\perp^2 + k_z^2$. We find two branches of the dispersion relation by inserting f_1 into (1) – (6). One branch is for the compressional mode

$$\omega^4 - k^2(c_s^2 + \frac{V_A^2}{1 + k^2\lambda_e^2})\omega^2 + k^2 k_z^2 \frac{c_s^2 V_A^2}{1 + k^2\lambda_e^2} = 0 \quad (14)$$

and the other branch is for the shear Alfvén mode (inertial Alfvén waves)

$$\omega^2 = \frac{k_z^2 V_A^2}{1 + k^2\lambda_e^2} \quad (15)$$

It can be seen that the compressional mode and the shear Alfvén mode are decoupled in the case of a uniform background even with the inclusion of electron inertia. In addition, there are dispersive effects for both the compressional mode and the shear Alfvén mode, because different wavenumber ($k_\perp$) components propagate at different velocities. Strong dispersion of the shear Alfvén mode occurs when $k_\perp$ increases significantly due to the narrowing of the resonance, as can be seen from (15). As to be shown in detail in the next section, the resonance narrows with time until it saturates due to loss mechanisms, such as electron inertia and the ionospheric Joule heating. On the other hand, the compressional mode does not show any very narrow structures, and the denominator in (14) is very close to unity. Therefore the dispersive effect on the compressional mode due to electron inertia is negligible. If electron inertia is ignored ($\lambda_e = 0$), the usual dispersion relationship for both the compressional mode and the shear Alfvén mode are recovered and there is no dispersive effect for the shear Alfvén mode.

In the present study, a simple rectangular box model of the three-dimensional magnetosphere is used. The x direction points radially toward Earth. The left boundary at $x = 0$ is the driver boundary, and the right boundary at $x = L_x$ is a boundary on the Earthward side of the resonance. The z direction points along the geomagnetic field lines. The bottom boundary at $z = 0$ is the ionosphere, and the top boundary at $z = L_z$ is the equatorial plane. The y direction is along the azimuthal ($\hat{\mathbf{z}} \times \hat{\mathbf{x}}$) direction. For simplicity we have assumed in the present study that the background magnetospheric plasma is cold ($\beta < m_e/m_i$) and the background magnetic field is constant. Therefore only nonuniformity in the plasma density is considered here. The result for the hot plasma with a nonuniform magnetic field will be presented in a separate paper. The plasma density decreases along the x direction and, consequently, the Alfvén velocity increases from the magnetopause toward Earth, as shown in Figure 1. In addition, the electron inertia length increases from the magnetopause toward Earth because it is also inversely proportional to the plasma density.

Generally speaking, to maintain the compressional mode and have a continuous excitation of the FLR, a constant monochromatic driver is required at the magnetopause. As discussed above, only discrete frequencies are sustained in a realistic magnetospheric cavity and each of these frequencies has a different resonant position. Therefore we assume for simplicity that the fast mode driver is a monochromatic compressional wave at the left boundary $x = 0$, which is inside the magnetosphere, greatly simplifying the driver boundary conditions at $x = 0$. Since electron inertia has little effect on the compressional mode, the dispersion relationship (14), which is required at $x = 0$, can be simplified by setting $\lambda_e = 0$. The frequency of the fast mode driver is the positive root of (14), which is

$$\omega_f^2 = \frac{1}{2}k^2(c_s^2 + V_A^2)(1 + \sqrt{1 - 4c_T^2 k_z^2/k^2}) \tag{16a}$$

where $k^2 = k_x^2 + k_y^2 + k_z^2$ and $c_T^2 = c_s^2 V_A^2/(c_s^2 + V_A^2)$, as defined previously. For a cold plasma $c_s = 0$ and $c_T = 0$, (16a) reduces to

$$\omega_f^2 = (k_x^2 + k_y^2 + k_z^2)V_A^2 \tag{16b}$$

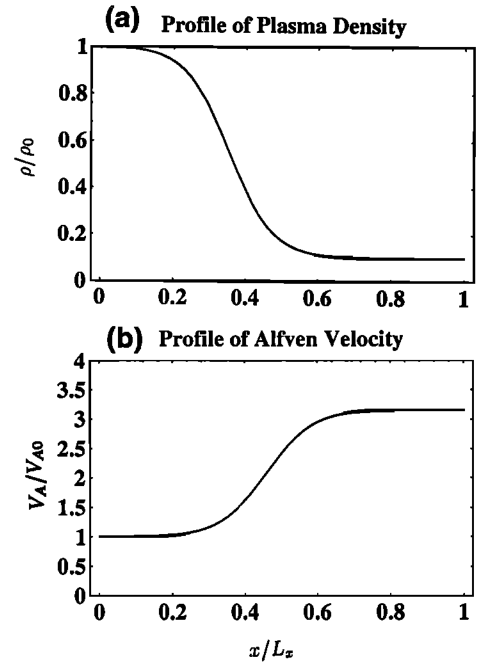

Figure 1. Initial profiles of (a) the plasma density and (b) the Alfvén velocity along the radial direction from the driver at the left boundary ($x = 0$) toward the Earthward boundary ($x = L_x$).

It can be seen that the frequency of the fast mode driver is determined by the physical parameters at the driver boundary ($x = 0$) and the wavenumber of the driver. For a given frequency of the driver, the physical components of the incident wave can be obtained by linearizing (7) – (10), under the assumption that the driver amplitude is relatively small compared with the zero-order fields.

In addition to the imposed fast mode driver which supplies energy into the simulation box from outside of the boundary, it is desirable that waves reflected from the turning point should be allowed to leave the system. To accomplish this, outgoing boundary conditions are applied at $x = 0$ for the reflected wave components. Therefore the boundary conditions at $x = 0$ consist of two parts: the imposed driver and the outgoing wave conditions. After some straightforward mathematical derivations, the boundary conditions at $x = 0$ can be expressed as

$$\frac{\partial f}{\partial t} - v_x \frac{\partial f}{\partial x} = 2\frac{\partial f_i}{\partial t} \tag{17}$$

where $f(x, y, z, t)$ is any one of the field variables corresponding to the waves, v_x is the perturbed x component velocity, and f_i is the imposed fast mode driver at $x = 0$. For the details of the mathematical derivations which lead to (17) as well as the expressions of f_i, we refer readers to *Rankin et al.* [1993b].

The ionospheric boundary conditions can be constructed in the same fashion. If the ionospheric conductivity is finite, partial reflection of waves at the ionosphere occurs and some wave energy is lost through Joule heating at the ionosphere. To handle this reflection, the boundary conditions for the wave field components at $z = 0$ are

$$(1-R)\frac{\partial f}{\partial t} - (1+R)v_z\frac{\partial f}{\partial z} = 0 \quad (18)$$

where R is the reflection coefficient at the ionosphere. Taking into account the electron inertial term in the magnetosphere gives

$$E_x/b_y = \pm\mu_0 V_A[1 + k_\perp^2\lambda_e^2]^{1/2} = \pm\Sigma_A^{-1} \quad (19)$$

In the usual way, considering an ionospheric slab with a height-integrated conductivity Σ_p, we have for the ionosphere

$$E_x/b_y = \Sigma_p^{-1} \quad (20)$$

Considering the incident and reflected waves gives

$$R = \frac{\Sigma_A - \Sigma_p}{\Sigma_A + \Sigma_p} \quad (21)$$

where Σ_A with electron inertia is given by (19). For a typical case with $\Sigma_p = 5$ mho and $V_A = 3 \times 10^4$ km/s, then $\Sigma_A(\text{no inertia}) \simeq 0.03$ mho and $R \simeq -0.99$. Including inertia leads to decrease of Σ_A, and therefore the reflectivity would be even higher. Bearing in mind that for such values of R ($|R| > 0.99$), the inertial effect on the reflection condition is negligible. We have chosen the reflection coefficient to be compatible with the above estimates and have not included the inertia correction since it is extremely small with the high reflectivity.

Boundary conditions at other surfaces are as follows. At the Earthward boundary $x = L_x$, a reflecting boundary condition is used. Symmetry conditions are applied at $z = L_z$ which is the equatorial plane. It can be shown that the plasma density ρ, the plasma pressure p, the parallel component of the magnetic field b_z, and the perpendicular components of the velocity v_x and v_y are symmetric with respect to $z = L_z$, while the perpendicular components of the magnetic field b_x and b_y and the parallel component of the velocity v_z are antisymmetric with respect to $z = L_z$. Periodic boundary conditions are used in the y direction.

Because of the different spatial scales and the large variation of the Alfvén velocity in the system, the restriction of the Courant-Friedrichs-Lewy condition [e.g., *Briley and McDonald*, 1977] for the time step makes it very difficult to use an explicit numerical scheme to solve (7) – (10). Consequently, we have developed an implicit numerical code, which uses the Douglas-Gunn algorithm [*Douglas and Gunn*, 1964] for alternating direction implicit temporal advancement, with an overall second-order accuracy in both space and time. The use of the alternating-direction implicit time steps allows the use of a time step that is many times larger than the time step in any explicit code [*Briley and McDonald*, 1977; *Finan and Killeen*, 1981]. In the three-dimensional case, the algorithm proceeds by advancing the system of equations along one spatial direction at a time, which involves the iterative solution of nonlinear block tridiagonal systems of algebraic equations. A major attraction of the Douglas-Gunn algorithm is that the intermediate solutions ψ^* (along the x direction) and ψ^{**} (along the y direction) are consistent approximations to the final solution ψ^{n+1} (along the z direction). We have implemented the alternating direction implicit algorithm on a four-processor Stardent 3040 computer on which it achieves near-ideal scaling from one to four processors. This machine is a small scale vector/parallel machine configured with four proprietary vector units, with an optimum performance of 128 million floating point operations per second when all processing elements are being utilized. We are in the process of implementing this code on a Myrias SPS-3 computer, which has 44 processors.

3. Simulation Results

In this section we present the simulation results for two different cases. In case A we show the results without electron inertial effects, while in case B, electron inertial effects are considered.

As pointed out earlier, the compressional wave suffers partial reflection at the turning point, and part of the compressional wave energy is coupled to the shear Alfvén wave at the resonance. This coupling process may be described by a coupling coefficient, which is defined as

$$q \simeq \frac{k_y^2}{(k_\parallel^2 V_A^2\, dV_A^{-2}/dx)^{2/3}} \quad (22)$$

It has been shown that, for a monochromatic wave, the coupling efficiency maximizes at $q \simeq 0.5$ [*Kivelson and Southwood*, 1986; *Inhester*, 1987]. In the simulation we choose wavenumbers k_y and k_z for the given Alfvén velocity profile to satisfy $q \sim 0.5$ near the resonance.

With consideration of the different spatial scales in the system, we have chosen $L_x \simeq 3200$ km, $L_y \simeq 6400$ km, and $L_z \simeq 1500$ km for the simulation box. The uniform background magnetic field is 5 nT. The background plasma density decreases from the magnetopause side toward Earth, as shown in Figure 1a. The plasma number density at the left boundary ($x = 0$) is $N_0 = 10^5$ m^{-3}. The above choice of the magnetic field and the plasma density gives an Alfvén velocity of $V_{A0} \simeq 345$ km/s at the left boundary. In our box the turning point is at $x_t \simeq 0.42\,L_x$ and the resonance without electron inertia is at $x_r \simeq 0.49\,L_x$. In the vicinity of the resonance, the plasma number density is about 0.2 N_0, and the Alfvén velocity is about 750 km/s or 2.2 V_{A0}, as shown in Figure 1. The electron inertia length along the x direction (not shown) has the same profile as the Alfvén velocity because they have exactly the same dependence on the plasma density in the case of a constant magnetic field. The electron inertia length is about 39 km at the position of the resonance. Note that from Figure 1a the plasma density is uniform near both the left and the right boundaries ($x = 0$ and $x = L_x$), such a choice of profile is mainly for the implementation of boundary conditions. In addition, we choose a very large magnetic Reynolds number ($R_m = 20{,}000$) to ensure numerical stability with little diffusion.

The normalized magnitude of the driver is two percent, which is the applied v_y at the left boundary $x = 0$. Other wave components can be obtained from the linearized set of equations. For example, the maximum driver for the azimuthal magnetic field b_y is about one percent, four percent for v_x, and two percent for b_x. The amplitude of the driver increases from zero to its maximum value linearly with time over a duration shorter than the Alfvén transit time in the box in order to allow a smooth initial setup.

Figure 2a shows a surface plot of the azimuthal magnetic field component b_y in the x-y plane at location $z = L_z/2$ and at time $t \simeq 3.0\,T_p$ in case A, in which electron inertial effects have been neglected. The time unit T_p is the wave period of the driver imposed at the left boundary $x = 0$. Note that b_y is predominantly due to the shear mode, and b_y will come only from the shear mode in cases where the compressional mode and the shear mode are decoupled. The amplitude of the driver at the left boundary ($x = 0$) is one percent, as can be seen from Figure 2a. Initially, there is no shear mode inside the system, and b_y is zero except at the left boundary where the driver is imposed. As time goes on, the standing wave structure of the compressional mode between the turning point and the magnetopause is gradually formed, and its amplitude increases with time due to the constant driver. At the same time, some portion of the compressional wave energy is coupled into the shear mode, which grows secularly. As shown in Figure 2a, the resonance structure is obvious at $x \simeq 0.49\,L_x$ by the time $t \simeq 3.0\,T_p$. The periodic y dependence of the driver at the left boundary ($x = 0$) and at the resonance is also evident in this figure.

Note that b_y is antisymmetric about the equatorial plane and symmetric about the ionosphere, yielding a maximum field-aligned current at the ionosphere. Therefore b_y has a node at the equatorial plane and an antinode at the ionosphere in such a case. The cuts at other locations along the z direction (not shown here) show profiles similar to that in Figure 2a, except that the amplitude increases from a minimum at the equator to a maximum at the ionosphere. Therefore the excited FLR is the fundamental mode. In addition, it is found that the v_y component has the same spatial profile as the b_y component along the x and y directions, consistent with properties of the shear Alfvén wave. However, v_y has an antinode at the equator and a node at the ionosphere, consistent with the fundamental mode structure. The amplitude of v_y decreases from its maximum at the equator to its minimum at the ionosphere.

Now we examine electron inertial effects. Figure 2b shows a surface plot of b_y in the x-y plane at location $z = L_z/2$ and at time $t \simeq 3.0\,T_p$ in case B, in which the electron inertial term has been included. It can be seen that Figures 2a and 2b are nearly identical. Therefore there is no significant electron inertial effect at this stage in the time evolution. The reason is that, although the FLR has formed due to mode coupling, the resonance width is still too large to be affected by electron inertia. All of the properties discussed for Figure 2a are also true here.

In an ideal magnetoplasma, coupling of the monochromatic, compressional driver leads to a shear Alfvén resonance which grows in amplitude and narrows with time due to phase mixing [*Poedts and Kerner*, 1992]. Saturation is reached when dissipation effects are included. Figures 3a and 3b show surface plots of b_y in the x-y plane at location $z = L_z/2$ and at time $t \simeq 7.5\,T_p$ in cases A and B, respectively. Comparing Figures 2 and 3, we can see that the amplitude of the FLR keeps increasing with time and, at the same time, the resonance narrows. At $t \simeq 7.5\,T_p$, the FLR has narrowed enough to be affected by electron inertia, as can be seen from Figure 3b. One noteworthy difference between Figures 3a and 3b is the additional set of peaks on the Earthward side of the resonance in Figure 3b. In addition, the main resonance peak has shifted Earthward in Figure 3b for the case with electron inertia, and the resonance width has also been broadened. These features can be seen more clearly from one-dimensional cuts along the x direction, which are shown below. The small variations which evolve on the driver side of the resonance in Figures 3a and 3b do not show in all of the simulation cases, and we plan further studies to determine the source of these variations.

Figure 4 shows one-dimensional cuts of the azimuthal magnetic field component b_y along the x direction at time $t \simeq 2.0\,T_p$ and at location $y \simeq 0.096\,L_y$ and $z = 0$. The dashed curve is a cut from case A, and the solid curve is a cut from case B. At this time the resonance width is

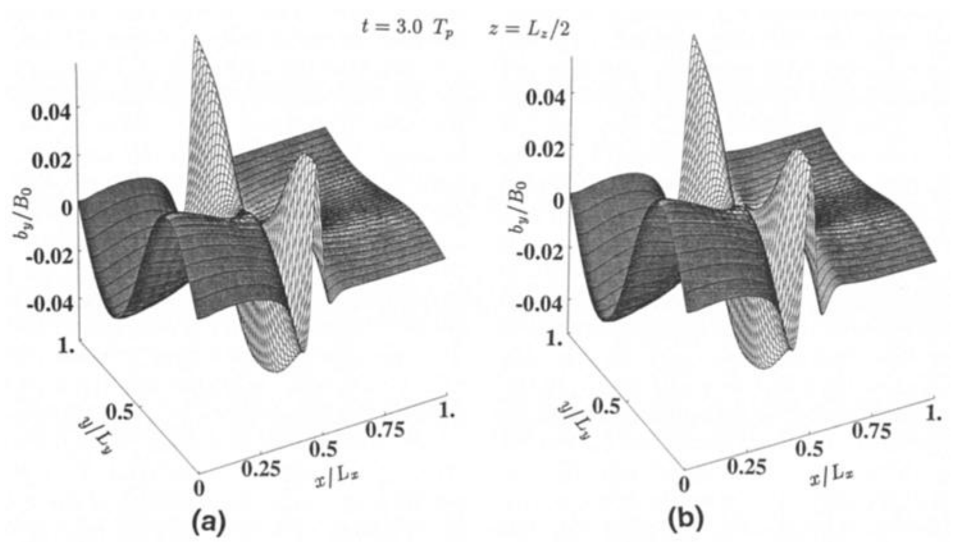

Figure 2. Azimuthal components of the perturbed magnetic field b_y at an early stage ($t \simeq 3.0\,T_p$, where T_p is the period of the driver) of the nonlinear evolution of FLRs. Shown here are surface plots at $z = L_z/2$, namely, halfway between the ionosphere and the equatorial plane. (a) Case A, (b) case B. The x direction is along the radial direction and points from the magnetopause toward Earth. The y direction is the azimuthal direction.

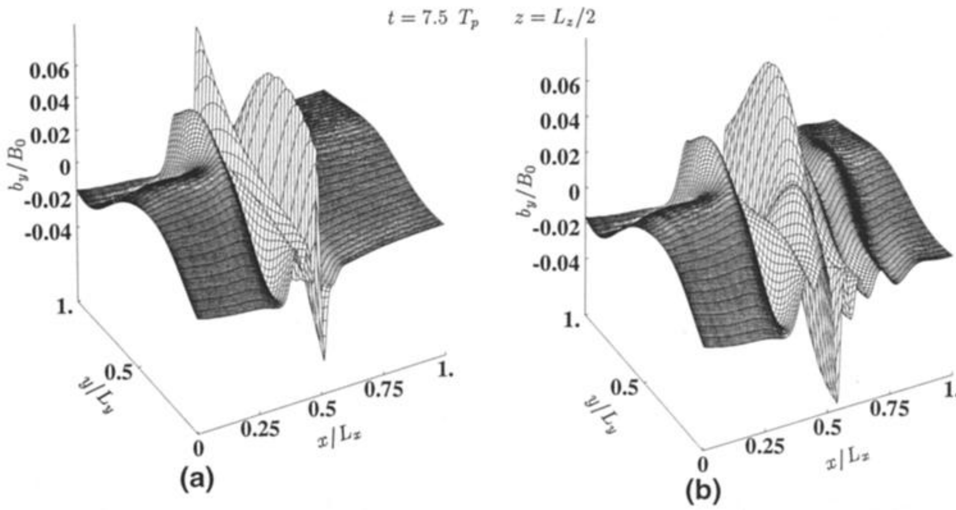

Figure 3. Similar to Figure 2 but at a later time $t \simeq 7.5\,T_p$.

$W_r \simeq 250$ km, which is defined as the distance between the half maxima. The ratio of the resonance width to the electron inertia length ($\lambda_e \simeq 39$ km at the resonance) is $W_r/\lambda_e \simeq 6.4$. As can be seen from Figure 4, although the resonance structure has formed at this stage, the resonance width is too large to allow discernible electron inertial effects.

Figure 5 shows the cuts at a later time $t \simeq 4.0\,T_p$ and at another location $y \simeq 0.064\,L_y$ and $z = 0$. As can be seen from the dashed curve (no electron inertia), the amplitude of b_y has increased with time, and the resonance width has become narrower than in Figure 4. The resonance width here is $W_r \simeq 110$ km, which gives $W_r \simeq 2.8\,\lambda_e$. However, the solid curve for the case with electron inertia is now substantially different from the case without electron inertia, indicating that electron inertial effects become important at this stage in the evolution of the FLR. We have run a large number of simulations with varied parameters and found that on average the dispersive effect of electron inertia become important when $W_r \leq 6\,\lambda_e$.

Further inspection of Figure 5 shows a number of the effects due to electron inertia, including the broadening of the resonance, an Earthward shift of the resonance peak, and the formation of an oscillating wavetrain on the Earthward side of the resonance (see also Figure 6). In fact, the profiles with electron inertia in Figures 5 and 6 are very similar in shape to the Airy function solutions expected when mode conversion to inertial Alfvén waves occurs in the linear regime.

The Earthward movement of the resonance peak can be understood by looking at the resonant condition with the electron inertia,

$$\omega^2 = \frac{k_z^2 V_A^2(x_r)}{1 + k_x^2 \lambda_e^2(x_r)} \tag{23}$$

where ω is the driver frequency. When λ_e is nonzero, the denominator in (23) increases, and for matching to occur, V_A must increase and the resonant position x_r must move Earthward.

Figure 6a shows a one-dimensional cut of b_y in case A along the x direction at time $t \simeq 8.0\,T_p$ and at location $y \simeq 0.78\,L_y$, $z = 0$, where b_y reaches its maximum. Figure 6b shows a one-dimensional cut of b_y in case B along the x direction at time $t \simeq 8.0\,T_p$ and at location $y = 0$ and $z = 0$, where b_y reaches its maximum. Because of the large dispersive effect of electron inertia near the resonance, the locations along the y direction where b_y reaches a maximum have different positions in cases A and

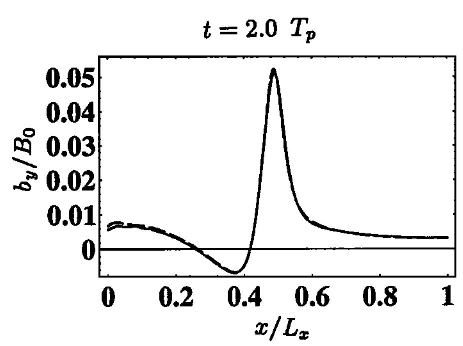

Figure 4. One-dimensional cuts of y components of the magnetic field b_y at the ionosphere at $t \simeq 2.0\,T_p$ along $y \simeq 0.096\,L_y$, where b_y reaches its maximum. The solid curve is for case B and the dashed curve is for case A.

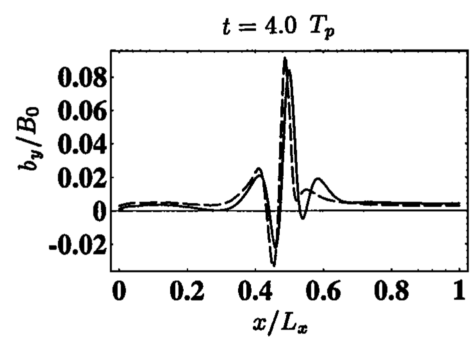

Figure 5. One-dimensional cuts of y components of the magnetic field b_y at the ionosphere at $t \simeq 4.0\,T_p$ along $y \simeq 0.064\,L_y$, where b_y reaches its maximum. The solid curve is for case B and the dashed curve is for case A.

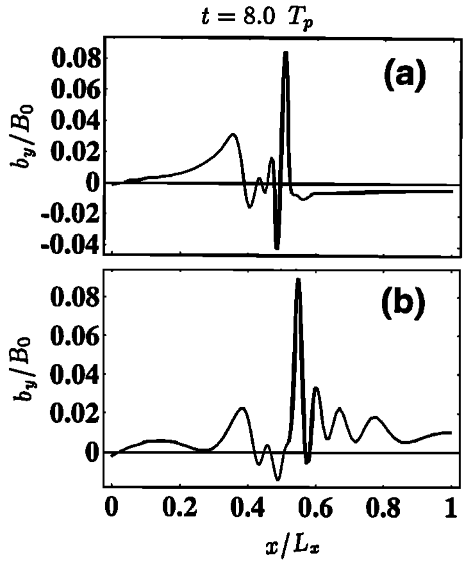

Figure 6. One-dimensional cuts of y components of the magnetic field b_y at the ionosphere at $t \simeq 8.0\,T_p$. (a) A cut at $y \simeq 0.78\,L_y$ for case A and (b) a cut at $y = 0$ for case B.

B. Therefore it is not appropriate to show Figures 6a and 6b together in one plot as we have done in Figures 4 and 5. A convenient way to represent these data is by using a Fourier transform along the y and z directions and then to compare the averaged amplitude at each x location (see Figure 7).

In Figure 6a the resonance has narrowed further at this time, and its amplitude has saturated due to the damping effect of the finite ionospheric conductivity. No further growth occurs after this time. The resonance width is $W_r \simeq 70$ km, which gives $W_r \simeq 1.8\lambda_e$. For the case with electron inertial effects as shown in Figure 6b, it can be seen that the resonance peak has shifted even farther Earthward and is located at $x \simeq 0.55\,L_x$, versus $0.50\,L_x$ in Figure 5.

The analysis of the three-dimensional plasma dynamics can be greatly simplified if we take advantage of the symmetries of the simulation box and use the Fourier transforms in the y and z directions. For each point in the x direction, a two-dimensional Fourier transformation is performed

$$f(x) = \iint f(x, y, z) \exp[i(k_y y + k_z z)]\, dy\, dz \qquad (24)$$

where k_y and k_z are wavenumbers associated with the driver and are the wavenumbers for the fundamental mode in the system ($k_y = 2\pi/L_y$ and $k_z = \pi/2L_z$).

Figures 7a, 7b, 7c, and 7d show the evolution of the Fourier amplitude (equation (24)) of the b_y component of the fundamental mode as a function of the x coordinate at times $t \simeq 2.0\,T_p$, $t \simeq 4.0\,T_p$, $t \simeq 6.0\,T_p$, and $t \simeq 8.0\,T_p$, respectively. As before, the solid curves are for case B and the dashed curves are for case A. At time $t \simeq 2.0\,T_p$ as shown in Figure 7a, the resonance is well formed and the peak is located at $x \simeq 0.49\,L_x$. The resonance width is large and electron inertial effects are negligible. As time goes on, the resonance width narrows and when the

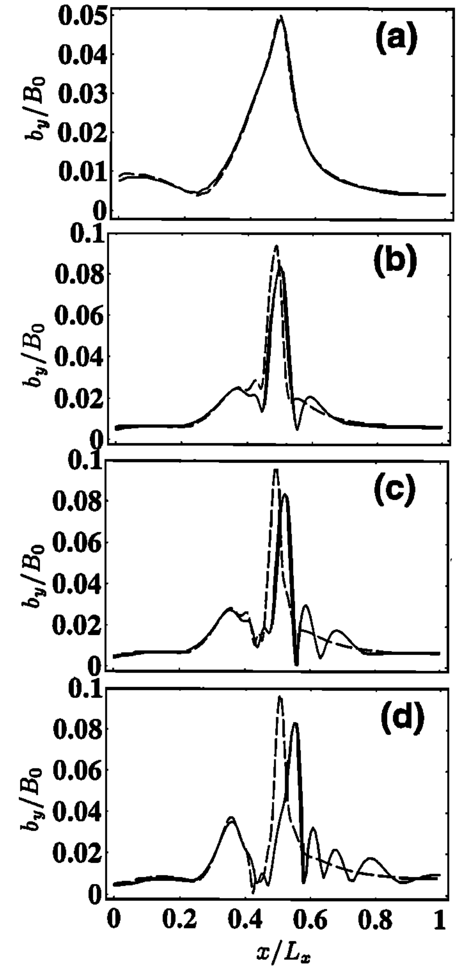

Figure 7. Time evolution of Fourier amplitude (Fourier transformation for all y and z) of the b_y component for the fundamental wave mode at (a) $t \simeq 2.0\,T_p$, (b) $t \simeq 4.0\,T_p$, (c) $t \simeq 6.0\,T_p$, and (d) $t \simeq 8.0\,T_p$, respectively. The solid curves are for case B and the dashed curves are for case A.

condition $W_r \leq 6\lambda_e$ is satisfied (Figure 7b), electron inertial effects modify the resonance structure. The resonance matching condition leads to an Earthward shift of the resonance for the case with electron inertia, and the dispersive effect leads to a lower peak amplitude, broadening of the resonance, and the propagation of energy Earthward from the resonance. When the resonance narrows further, the dispersive effect becomes stronger, as can be seen from Figure 7c. Eventually, the system reaches saturation (Figure 7d).

In addition to the shear Alfvén mode studied above, the compressional mode can be studied by examining other components of the wave field. Figures 8a, 8b, 8c, and 8d show Fourier components of b_x, b_z, v_x, and ρ, respectively, for the fundamental wave mode at time $t \simeq 6.0\,T_p$ along the x direction. The solid curves are for case B and the dashed curves are for case A. Note that the uniform background values of the plasma density and the magnetic field have been subtracted while performing the Fourier transformation to get Figures 8b and 8d. These plots show that electron inertia has little effect on the fast mode either at the turning point ($x \simeq 0.42\,L_x$) or at the resonance

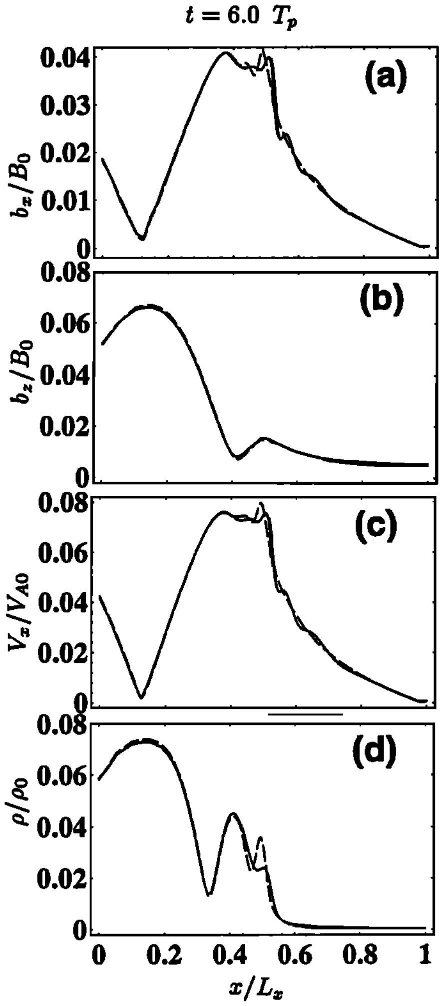

Figure 8. Fourier amplitude of (a) b_x, (b) b_z, (c) v_x, and (d) ρ for the fundamental wave mode at time $t \simeq 6.0\,T_p$. The solid curves are for case B and the dashed curves are for case A.

(except for small differences in the plasma density ρ). Therefore it can be concluded that the electron inertial effect, if any, would mainly affect the resonance structure, namely, the shear Alfvén mode. In addition, it can be seen from Figures 8a and 8c that b_x and v_x have little variations across the turning point and rapidly decrease to zero beyond the resonance. These two components are a mixture of the shear mode and the compressional mode. The other two components, b_z and ρ as shown in Figures 8b and 8d, diminish beyond the turning point and they are mainly due to the fast mode. The sharp decrease of the amplitude here is an indication that the fast mode energy has been absorbed by the resonance due to mode conversion.

We have also looked for manifestations of nonlinear effects in the FLRs and find that for both cases A and B there are density fluctuations near the equator. The density grows with time but has superposed oscillations at the driver frequency ω_0 and at $2\,\omega_0$. The $2\,\omega_0$ fluctuations indicate that nonlinear ponderomotive forces [*Allan*, 1992] are playing a role in the evolution of the FLR. Nevertheless, in this simulation, mode conversion to inertial Alfvén waves seems to play the dominant role in saturating the growth of the FLR. We are planning further studies to look at the competing effects of mode conversion and nonlinear harmonic generation in the saturation of FLRs.

A number of studies have suggested that inertial or kinetic effects in FLRs might lead to electron heating and acceleration and the formation of auroral arcs [*Hasegawa*, 1976; *Samson et al.*, 1991; *Xu et al.*, 1993]. To illustrate this possibility with the present simulation results, we have estimated the field-aligned current from the z component of $\nabla \times \mathbf{B}$ and the parallel component of the electric field. Figure 9 shows a one-dimensional cut of the field-aligned current density J_z (the solid curve) at the ionosphere at $t \simeq 8.0\,T_p$ along $y \simeq 0.25\,L_y$ for case B, together with the b_y component of the magnetic field at the same position (the dashed curve) for comparison. Positive J_z indicates upward field-aligned current from the ionosphere toward the equatorial plane. Only the positive field-aligned current regions would be expected to lead to the acceleration of electrons and the formation of auroral arcs. The maximum field-aligned current density in this case is $\sim 0.018\ \mu$A/m^2. Our model does not include the convergence of dipolar magnetic field, and, consequently, this number is only a rough lower bound for the currents that might be expected in the magnetosphere. The major contribution to the field-aligned current comes from the variation of the azimuthal magnetic field in the radial direction.

Figure 10a shows a contour plot of the parallel electric field in the x-z plane near $y = L_y$ at $t \simeq 7.5\,T_p$ for case B with the inclusion of electron inertia. Solid lines are for positive fields and dashed lines are for negative fields. The contour interval is about 0.002 mV/m. Note that the spatial interval along the x direction is nonuniform, and the portion near the resonance is greatly enlarged in order to show more clearly the contour pattern. Figure 10a shows that the maximum value of the parallel electric field is located near the ionosphere at the resonance peak, and its maximum value is about 0.021 mV/m, while its minimum value is about -0.013 mV/m. In addition, the dispersive effects of electron inertia add considerable spatial structures. This structure might be associated with the thinner discrete arcs (kilometers in thickness) which are embedded in the larger scale (tens of kilometers) in inverted V structures. The solid curve in Figure 10b shows a one-dimensional cut

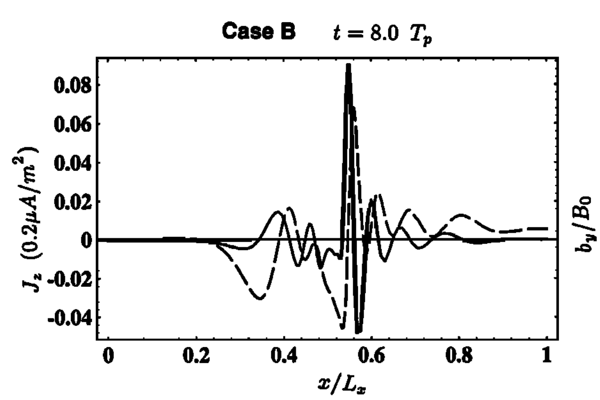

Figure 9. A one-dimensional cut of the field-aligned current density J_z (solid curve) and the y component of the magnetic field b_y (dashed curve) at the ionosphere at $t \simeq 8.0\,T_p$ along $y \simeq 0.25\,L_y$ in Case B. Positive J_z indicates upward field-aligned currents.

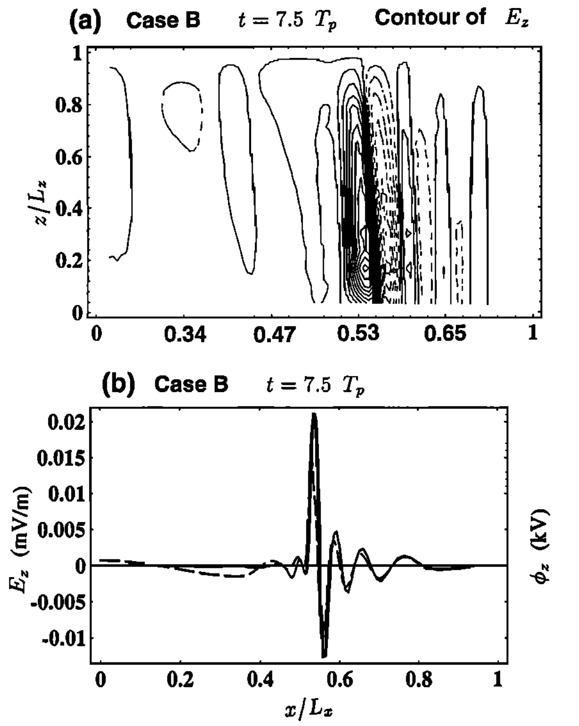

Figure 10. (a) Contour plot of the parallel electric field in the x-z plane near $y = L_y$ at $t \simeq 7.5 T_p$ in case B. The solid lines are for positive values and the dashed lines are for negatives values. The contour interval is about 0.002 mV/m. Note that the spatial interval along the x direction is nonuniform. (b) One-dimensional cuts of the parallel electric field E_z near the ionosphere (solid curve) and the field-aligned potential drop ϕ_z at the ionosphere (dashed curve).

of the parallel electric field E_z at $z \simeq 0.14 L_z$ where E_z reaches its maximum. The E_z profile is similar to the field-aligned current profile in Figure 9. The dashed curve in Figure 10b shows the field-aligned potential drop (the integrated E_z in the z direction) at the ionosphere. The maximum field-aligned potential drop is about 15 V at the resonant position.

While a parallel potential drop $\delta\phi_{\parallel}$ of 15 V seems very small, we note that in our simulations the radial potential drop from the center of the resonance to the first zero of the electric field in the equatorial plane $\delta\phi_{\perp}$ is of the order of 30 V. Consequently, $\delta\phi_{\parallel}/\delta\phi_{\perp} \simeq 0.5$. Observed equatorial velocity fields of FLRs in the magnetosphere are of the order of 200 km/s at 8 to 10 R_E, and the resonance might have a half width of $\sim 0.1\ R_E$, giving an observed $\delta\phi_{\perp}$ of about 8 keV. On the basis of the ratio $\delta\phi_{\parallel}/\delta\phi_{\perp}$ in our simulation, we find that an order of magnitude estimated from $\delta\phi_{\parallel}$ in the magnetosphere is about 4 keV. These energies are typical of those found in discrete auroral arcs.

4. Discussion and Conclusions

FLRs in Earth's magnetosphere can be saturated due to a number of physical mechanisms. In the linear regime, dissipation of energy by Joule heating in the ionosphere and mode conversion to kinetic or inertial Alfvén waves stabilize the resonance at finite widths and amplitudes. In the nonlinear regime, harmonic generation (including nonlinear ponderomotive forces) and other nonlinear effects such as the Kelvin-Helmholtz instability in the equatorial plane [*Samson et al.*, 1992; *Rankin et al.*, 1993a] can dissipate the energy in the resonance. The variety of possibilities is clearly large, and a code used for studying the evolution of FLRs must be able to accommodate the possible nonlinear effects. In our simulation, mode conversion dominates the dissipation in the FLR, though nonlinear effects are apparent.

Our simulation results indicate that mode conversion to inertial Alfvén waves becomes important when the width of the resonance is of the order of $6\,\lambda_e$. Measurements of FLRs in the ionosphere [*Walker et al.*, 1992] and estimates of the widths of FLRs based on the typical ionospheric conductivities (without electron inertia [*Rankin et al.*, 1993b]) indicate that the widths in the auroral ionosphere might be less than 20 − 30 km ($\sim 0.1\ R_E$ in the equatorial plane). These widths map to several electron inertia lengths at 1.5 to 2 R_E above the auroral ionosphere, indicating that inertial effects might play a role in some FLRs in Earth's magnetosphere. The results from our simulation are compatible with this possibility. Furthermore, our simulation results show that the resonance narrows enough to allow inertial effects within approximately five wave cycles. The wave-trains of many FLRs are much longer than this [*Walker et al.*, 1992].

The net field-aligned potentials in our simulation are compatible with those estimated by *Borovsky* [1993] for electron inertial effects. Borovsky showed that the arc should have a width of approximately $2\,\pi\lambda_e$ and

$$\delta\phi_{\parallel} = \frac{k_{\perp}^2\lambda_e^2}{1 + k_{\perp}^2\lambda_e^2}\delta\phi_{\perp} \tag{25}$$

In our simulations we have shown that when electron inertia is important, the width of the resonance is of the order of $6\,\lambda_e$ ($\sim 2\,\pi\lambda_e$) or equivalently $k_{\perp}\lambda_e \simeq 1$ ($\lambda \simeq 2\,\pi\lambda_e$), giving $\delta\phi_{\parallel}/\delta\phi_{\perp} \simeq 0.5$ according to (25). Such an estimation is very close to our measured value.

Even though more sophisticated simulations with dipolar configurations and realistic plasma densities and pressures are needed, our results show that the relatively simple and eloquent mechanism of mode conversion might lead to the formation of some auroral arcs. The only requirements of the model are a nonuniform magnetoplasma and a source of monochromatic compressional waves. Potential sources of these monochromatic waves are cavity modes [*Kivelson and Southwood*, 1986] and waveguide modes [*Samson et al.*, 1992]. The coupling of the compressional to shear Alfvén waves forms FLRs on magnetic shells. These FLRs narrow with time, and if ionospheric conductivity is high enough, electron inertial effects become important, with mode conversion to inertial Alfvén waves. The width of the resonance is determined by electron inertia, giving $\delta\phi_{\parallel} \simeq 0.5\,\delta\phi_{\perp}$. Observed FLRs have $\delta\phi_{\perp} \simeq$ several keV, allowing field-aligned potential drops (and accelerated electrons) of a number of keV. If we assume that λ_e at $1.5 - 2\ R_E$ determines the effective width of the resonance, the latitudinal width in the ionosphere would be about 10 − 20 km.

Much remains to be done in numerical computational studies of the evolution of FLRs. More realistic (dipolar) geometries are needed as we consider finite β effects. The competition among ionospheric dissipation, mode conversion, and nonlinear effects must be taken into account. We have been able to show that in some cases mode conversion is the dominant mechanism for saturation and stabilization of the FLRs. In the nonlinear regime we must consider harmonic generation and nonlinear instabilities such as localized tearing modes and equatorial Kelvin-Helmholtz instabilities. We are presently testing models which show strong harmonic generation and ponderomotive forces when electron inertial effects are not important.

The simulation results presented in this paper indicate that there are large azimuthal components of the magnetic field near the ionosphere and in the velocity near the equatorial plane associated with inertial Alfvén waves. The large azimuthal magnetic field leads to a large field-aligned current, which might excite localized tearing mode instabilities and hence lead to the formation and structuring of some auroral arcs. The localized tearing mode should evolve in the nonlinear regime when electron inertia and the large field-aligned currents in the resonance near the ionosphere are taken into account (measured currents may be greater than 5 μA/m^2). Here the scenario is very similar to the auroral arc model considered by *Seyler* [1990].

The nonlinear Kelvin-Helmholtz instability evolves in the equatorial plane because of the large velocity shears in this region of the FLR. *Rankin et al.* [1993a] have shown that this instability occurs in models which are initialized with the fields of an FLR. We are now looking for these instabilities in driven FLRs like the one in this study.

By using a boxlike model of the magnetosphere, we have neglected the convergence of the geomagnetic field. As a consequence, all of the physical quantities which involve a mapping between the magnetosphere and the ionosphere cannot be quantitatively compared with observations. Therefore the values for the field-aligned current, the parallel electric field, and the field-aligned potential drop obtained in the previous section are only qualitative. Nevertheless, the present model provides a global picture of FLRs when electron inertial effects are included. It leads to a better understanding of mode conversion from compressional waves to shear Alfvén waves and the energy transfer from the driver into the system and consequently conversion into field-aligned oscillations. It shows clearly the dispersive effect of electron inertia. It gives profiles of the parallel electric field and the field-aligned potential drop, which would not be present if electron inertia is neglected.

The principal results of this paper may be summarized as follows:

The coupling of fast mode compressional waves to shear Alfvén waves leads to the formation of large-amplitude FLRs near Earth where the frequency of the fast mode driver wave matches the local Alfvén wave frequency. The FLR may reach saturation within several wave periods.

The dispersive effect of electron inertia becomes important to the resonance structures when the resonance narrows to about six electron inertia lengths ($W_r \leq 6\,\lambda_e$). The electron inertial effect is more significant when the FLR width narrows further.

Dispersive effects of electron inertia lead to several new effects. These include the broadening of the resonance, an Earthward shift of the resonance peak, and the formation of a spatially oscillating wavetrain on the Earthward side of the resonance. The final profiles of the resonance are very similar in shape to the Airy function solutions for linear mode conversion problems.

Inclusion of electron inertia has little effect on the compressional mode because electron inertia does not significantly modify the wavenumber in the region where the fast mode wave is dominant.

A number of linear and nonlinear mechanisms may lead to saturation of FLRs. The linear mechanisms are dissipation of energy by Joule heating in the ionosphere and mode conversion to kinetic or inertial Alfvén waves, while harmonic generation (including nonlinear ponderomotive forces) and the Kelvin-Helmholtz instability are possible nonlinear mechanisms.

Parallel electric fields associated with inertial Alfvén waves with inclusion of electron inertia lead to the existence of field-aligned potential drops between the equatorial plane and the ionosphere. These potential drops may lead to the acceleration of electrons in the auroral region and the formation of some types of auroral arcs.

Acknowledgments. The work is supported by the Canadian Network for Space Research under the Networks of Center of Excellence Program.

The Editor thanks R. L. Lysak and E. A. Bering for their assistance in evaluating this paper.

References

Allan, W., Ponderomotive mass transport in the magnetosphere, *J. Geophys. Res.*, *97*, 8483, 1992.

Allan, W., and E. M. Poulter, ULF waves — Their relationship to the structure of the Earth's magnetosphere, *Rep. Prog. Phys.*, *55*, 533, 1992.

Allan, W., E. M. Poulter, and S. P. White, Hydromagnetic wave coupling in the magnetosphere-plasmapause effects on impulse-excited resonance, *Planet. Space Sci.*, *12*, 1189, 1986.

Borovsky, J. E., Auroral arc thickness as predicted by various theories, *J. Geophys. Res.*, *98*, 6101, 1993.

Briley, W. R., and H. McDonald, Solution of the multidimensional compressible Navier-Stokes equations by a generalized implicit method, *J. Comput. Phys.*, *24*, 372, 1977.

Chen, L., and A. Hasegawa, A theory of long-period magnetic pulsations, 1, Steady excitation of field line resonances, *J. Geophys. Res.*, *79*, 1024, 1974a.

Chen, L., and A. Hasegawa, A theory of long-period magnetic pulsations, 2, Impulse excitation of surface eigenmode, *J. Geophys. Res.*, *79*, 1033, 1974b.

Cummings, W. D., R. J. O'Sullivan, and P. J. Coleman, Jr., Standing Alfvén waves in the magnetosphere, *J. Geophys. Res.*, *74*, 778, 1969.

Douglas, J., and J. Gunn, A general formulation of alternating direction methods. I. Parabolic and hyperbolic problems, *Numer. Math.*, *6*, 428, 1964.

Finan, C. H., III, and J. Killeen, Solution of the time-dependent, three-dimensional resistive magnetohydrodynamic equations, *Comput. Phys. Commun.*, *24*, 441, 1981.

Goertz, C. K., Kinetic Alfvén waves on auroral field lines, *Planet. Space Sci.*, *32*, 1387, 1984.

Harrold, B. G., and J. C. Samson, Standing modes of the magnetosphere: A theory, *Geophys. Res. Lett.*, *19*, 1811, 1992.

Hasegawa, A., Particle acceleration by MHD surface wave and formation of aurora, *J. Geophys. Res.*, *81*, 5083, 1976.

Hasegawa, A., and L. Chen, Kinetic processes in plasma heating by resonant mode conversion of Alfvén waves, *Phys. Fluids*, *19*, 1924, 1976.

Hughes, W. J., R. L. McPherron, and J. N. Barfield, Geomagnetic pulsations observed simultaneously on three geostationary satellites, *J. Geophys. Res.*, *83*, 1109, 1978.

Inhester, B., Numerical modeling of hydromagnetic wave coupling in the magnetosphere, *J. Geophys. Res.*, *92*, 4751, 1987.

Kivelson, M. G., and D. J. Southwood, Resonant ULF waves: A new interpretation, *Geophys. Res. Lett.*, *12*, 49, 1985.

Kivelson, M. G., and D. J. Southwood, Coupling of global magnetospheric MHD eigenmode to field line resonances, *J. Geophys. Res.*, *91*, 4345, 1986.

Lee, D.-H., and R. L. Lysak, Magnetospheric ULF wave coupling in the dipole model: The impulsive excitation, *J. Geophys. Res.*, *94*, 17,097, 1989.

Lee, D.-H., and R. L. Lysak, Impulsive excitation of ULF waves in the three-dimensional dipole model: The initial results, *J. Geophys. Res.*, *96*, 3479, 1991.

Lee, L. C., and C. Q. Wei, Interaction of solar wind with the magnetopause-boundary layer and generation of magnetic impulse events, *J. Atmo. Terr. Phys.*, *55*, 967, 1993.

Lysak, R. L., Electrodynamic coupling of the magnetosphere and the ionosphere, *Space Sci. Rev.*, *52*, 33, 1990.

Poedts, S., and W. Kerner, Time scales and efficiency of resonant absorption in periodically driven resistive plasmas, *J. Plasma Phys.*, *47*, 139, 1992.

Rankin, R., B. G. Harrold, J. C. Samson, and P. Frycz, The nonlinear evolution of field line resonances in the Earth's magnetosphere, *J. Geophys. Res.*, *98*, 5839, 1993a.

Rankin, R., J. C. Samson, and P. Frycz, Simulations of driven field line resonances in the Earth's magnetosphere, *J. Geophys. Res.*, *98*, 21,341, 1993b.

Roberts, B., Waves in inhomogeneous media, *Eur. Space Agency Spec. Publ.*, *ESA SP-220*, 137, 1984.

Samson, J. C., Three-dimensional polarization characteristics of high-latitude Pc 5 geomagnetic micropulsations, *J. Geophys. Res.*, *77*, 6145, 1972.

Samson, J. C., T. J. Hughes, F. Creutzberg, D. D. Wallis, R. A. Greenwald, and J. M. Ruohoniemi, Observation of a detached discrete arc in association with field line resonances, *J. Geophys. Res.*, *96*, 15,683, 1991.

Samson, J. C., B. G. Harrold, J. M. Ruohoniemi, R. A. Greenwald, and A. D. M. Walker, Field line resonances associated with MHD waveguides in the magnetosphere, *Geophys. Res. Lett.*, *19*, 441, 1992.

Seyler, C. E., A mathematical model of the structure and evolution of small-scale discrete auroral arcs, *J. Geophys. Res.*, *95*, 17,199, 1990.

Singer, H. J., W. J. Hughes, and C. T. Russell, Standing hydromagnetic waves observed by ISEE 1 and 2: Radial extent and harmonic, *J. Geophys. Res.*, *87*, 3519, 1982.

Southwood, D. J., Some features of field line resonances in the magnetosphere, *Planet. Space Sci.*, *22*, 483, 1974.

Southwood, D. J., and W. J. Hughes, Theory of hydromagnetic waves in the magnetosphere, *Space Sci. Rev.*, *35*, 301, 1983.

Walker, A. D. M., R. A. Greenwald, A. Korth, and G. Kremser, STARE and GEOS 2 observations of a storm time Pc 5 ULF pulsation, *J. Geophys. Res.*, *87*, 9135, 1982.

Walker, A. D. M., J. M. Ruohoniemi, K. B. Baker, R. A. Greenwald, and J. C. Samson, Spatial and temporal behavior of ULF pulsations observed by the Goose Bay HF radar, *J. Geophys. Res.*, *97*, 12,187, 1992.

Xu, B.-L., J. C. Samson, W. W. Liu, F. Creutzberg, and T. J. Hughes, Observations of optical aurora modulated by resonant Alfvén waves, *J. Geophys. Res.*, *98*, 11,531, 1993.

Yumoto, K., External and internal sources of low-frequency MHD waves in the magnetosphere: A review, *J. Geomagn. Geoelectr.*, *40*, 293, 1988.

Zhu, X., and M. G. Kivelson, Analytic formulation and quantitative solutions of the coupled ULF wave problem, *J. Geophys. Res.*, *93*, 8602, 1988.

P. Frycz, R. Rankin, J. C. Samson, and C. Q. Wei, Canadian Network for Space Research, CW-005 Biological Sciences Building, University of Alberta, Edmonton, Alberta, Canada T6G 2E9. (email: cqwei@space.ualberta.ca)

(Received September 13, 1993; revised January 3, 1994; accepted February 17, 1994.)